Pergamon

Geochimica et Cosmochimica Acta, Vol. 67, No. 5, pp. 831–843, 2003

0016-7037/03 $30.00 + .00

PII S0016-7037(02)01146-8

A comparison of the dissolution behavior of troilite with other iron(II) sulfides; implications of structure

JOAN E. THOMAS,* WILLIAM M. SKINNER, and ROGER ST. C. SMART
Ian Wark Research Institute, University of South Australia, Mawson Lakes, South Australia 5095, Australia

(*Received November* 26, 2001; *accepted in revised form August* 19, 2002)

Abstract—Further knowledge as to the nature of the structure of a terrestrial sample of troilite, FeS [stoichiometric iron(II) sulfide] is revealed by a combination of XPS studies and dissolution studies in acid. The XPS analysis of a pristine troilite surface (the sample being cleaved under high vacuum) is compared to that of a surface polished in an inert atmosphere and a surface after reaction in deoxygenated acid. Further comparison is made with polished and acid-reacted surfaces of pyrrhotite ($Fe_{1-x}S$) and pyrite (FeS_2). The pristine troilite S2*p* spectrum comprises mainly monosulfide 161.1 eV, within the reported range of monosulfide, together with evidence of an unsatisfied monosulfide surface state arising from S–Fe bond rupture. Small, higher oxidation state sulfur contributions, including a disulfide-like state are also present, which suggest the presence of defects due to some nonstoichiometry. The dissolution studies showed that the troilite, in addition to dissolving in acid as an ionic solid to produce H_2S, also exhibits some oxidation of sulfur in the surface layers. In addition, a study of the dissolution behavior of troilite under the influence of cathodic applied potential supported the existence of a proportion of the sulfur within troilite needing reduction before dissolution forming HS^- or H_2S can occur. A significant increase in the dissolution rate was observed with application of −105 mV (SHE), but further stepped decreases in potential to −405 mV and −705 mV resulted in a decreased rate of dissolution, a response typical of an ionic solid. The results of the studies emphasise the viewing of iron(II) sulfides as a continuum. Pyrrhotite has been reported previously to dissolve in acid both oxidatively (like pyrite) and nonoxidatively (like troilite) on the same surface. Dissolution studies using troilite, in Ar-purged acid, indicate that dissolution of this material may not be uniformly nonoxidative. XPS evidence of restructuring of the surface of troilite to pyrrhotite and the surface of pyrrhotite towards a FeS_2 type structure, after exposure to Ar-purged acid, is presented.

1. INTRODUCTION

Iron forms a variety of binary compounds with sulfur. These range from stoichiometric FeS_2, pyrite and marcasite, through a range of nonstoichiometric compounds, classed as pyrrhotite, $Fe_{1-x}S$, which have an excess of sulfur over iron, to stoichiometric FeS, troilite, and to metal rich (sulfur deficient) mackinawite (FeS_{1-x}) (Kostov and Minceva-Stefanova, 1982). Troilite, stoichiometric FeS, is a rare mineral, formed in nature under strongly reducing conditions (Evans, 1970). One such reducing environment is in swamps, where anaerobic bacteria can reduce sulfate to sulfide. Studies of swamp sediment by Luther III showed only low concentrations (if at all) of iron monosulfides, but an abundance of framboidal or finely crystalline pyrite. Rickard (1974, 1975) studied the formation of iron monosulfides from goethite and soluble sulfide, and their subsequent further reaction with sulfur to form pyrite. It is recognized that the transformation of pyrrhotite to pyrite (FeS_2) does not occur directly. Marcasite (FeS_2) (a polymorph of pyrite), or a mixture of marcasite and pyrite, is commonly found as the replacement product for pyrrhotite in a supergene environment. The structural reorganization necessary for pyrrhotite to transform to marcasite is less complex than that required for the transformation to pyrite (Fleet, 1978).

Goodenough (1982) points out that a very limited deficiency of iron ($Fe_{1-\delta}S$ where $0 < \delta < 0.055$) is possible for troilite. Goodenough (1982) and Vaughan and Craig (1978), allow the possibility that troilite may contain more than one phase, albeit phases that are very closely related. These variations may include some slight changes from stoichiometry with possible iron rich and iron deficient regions, possibly due to disproportionation, or inhomogeneity during formation.

Troilite, stoichiometric iron(II) monosulfide (FeS), has a hexagonal close packed structure with FeS_6 and SFe_6 units. Troilite at temperatures below 140 °C has distortions from the ideal (NiAs) hexagonal structure. The crystallographic designation for troilite is hexagonal with a superstructure designation of 2C. The "c" dimension of the unit cell is twice the "c" dimension of the ideal NiAs structure (Vaughan and Craig, 1978).

Both lunar and terrestrial troilite show distortions from ideal lattice positions, triangular groupings of iron atoms are displaced in the *x–y* plane forming contracted and dilated triangular units. The sulfur network is much less distorted with only a slight displacement of one-third of the sulfur atoms along the *c* axis, away from the center of the Fe triangles. The distorted FeS_6 units have six different Fe–S bond lengths ranging from 2.359 Å to 2.721 Å (Bertaut, 1956; Evans, 1970).

Pyrrhotite is the name given to a range of nonstoichiometric compounds intermediate to the stoichiometric extremes of troilite and pyrite. Pyrrhotite has an excess of sulfur over iron and is described by the general formula $Fe_{1-x}S$, where the values of x vary within the range $0 < x < 0.125$. The structure of pyrrhotite varies from hexagonal to monoclinic, with increasing iron deficiency. The nonstoichiometry of pyrrhotite arises from

* Author to whom correspondence should be addressed (joan.thomas@unisa.edu.au).

iron vacancies distributed throughout the lattice (Posfai and Dodonay, 1990; Tokonamai et al., 1972). Pyrrhotite has recently been shown to contain both Fe(II)–S and Fe(III)–S, from studies on pyrrhotite surfaces exposed by fracture within the evacuated XPS analysis chamber (Pratt et al., 1994).

The importance of the structure of the mineral, rather than just the type of atoms involved, is highlighted by the variable dissolution behavior of the iron sulfides. In acidic solution iron sulfides exhibit both nonoxidative dissolution, releasing iron ions into solution with the production of $HS^-_{(aq)}$ and $H_2S_{(g)}$ and oxidative dissolution which releases Fe^{2+} and SO_4^{2-} ions into solution. Observed dissolution rates in pH 1 acid (under closely matched conditions) range over 5 orders of magnitude, from 10^{-4} mol m^{-2} s^{-1} for troilite to 10^{-9} mol m^{-2} s^{-1} for pyrite (Thomas et al., 2000). Troilite dissolves nonoxidatively (Eqn. 1) while pyrite dissolves oxidatively (Eqn. 2). With troilite dissolution, the resulting sulfide ion consumes acid to form HS^- or H_2S (depending on the pH). At a pH of 1, H_2S is formed as described by Eqn. 1. The oxidative dissolution of pyrite (Eqn. 2) is an acid producing reaction and has long been identified as the main source of acid leachate from mineral deposits, particularly those disturbed by mining,

$$FeS + 2H^+ \rightarrow Fe^{2+} + H_2S, \quad (1)$$

$$FeS_2 + 8H_2O \rightarrow Fe^{2+} + 2SO_4^{2-} + 16H^+. \quad (2)$$

Pyrrhotite has been shown to exhibit both oxidative and nonoxidative dissolution. Thomas et al. (1998) identified four distinct stages of dissolution that may occur with pyrrhotite. A reduction mechanism allowing oxidative dissolution to change to nonoxidative dissolution has been proposed (Thomas et al., 2001). This reduction mechanism involves a limited accumulation of electrons within a surface state of pyrrhotite.

The oxidative dissolution of iron sulfides is at least 10^3 times slower than nonoxidative dissolution. Thus, the reaction kinetics of a system will be dominated by nonoxidative dissolution even if only a small proportion of the surface is dissolving in this manner. Only S^{2-} reacts to form H_2S when in contact with acid, regardless of the presence of oxidizing species. Covalent S–S bonding (polysulfides, including disulfide) require reduction before HS^- or H_2S can be produced. Oxidative dissolution occurs in the presence of oxidizing agents, including dissolved O_2 or Fe(III) ions. In the case of pyrrhotite, iron was shown to be released into solution at a faster rate than sulfate, resulting in an increasingly sulfur rich surface layer (Thomas et al., 1998).

Studies with troilite were done to investigate the differences in the bonding of the surface layers of the stoichiometric material with that found in pyrrhotite (nonstoichiometric due to iron deficiency). Surface studies using XPS were used to follow changes in the bonding of Fe and S from that found in a pristine (vacuum cleaved) surface, to that found on a surface polished in preparation for dissolution studies. These results were compared with the state of Fe and S on an initially polished surface that had undergone leaching in deoxygenated acid. The surfaces of acid reacted pyrrhotite and pyrite were also investigated using XPS. The restructuring of pyrrhotite, after leaching in Ar-purged acid, towards a FeS_2 type structure had previously been proposed by Jones et al. (1992) on the basis of XRD evidence of a new phase in acid-reacted pyrrhotite powder. Within this phase a sulfur sub-lattice was proposed which consists of linear arrays of sulfur atoms with a bond length similar to S_8.

To complement the surface studies, the differences in the bonding within troilite, pyrrhotite, and pyrite was investigated by studying the response of polished discs of troilite, pyrrhotite, and pyrite to an applied cathodic potential. If the sulfur within the iron (II) sulfide were entirely monosulfide, then such a potential would decrease the reaction rate by adding an additional energy barrier for the release of S^{2-}. If covalent S–S bonding is present, a cathodic potential will enhance the formation of S^{2-} and thus increase nonoxidative dissolution, which will in turn increase the rate of dissolution.

2. METHOD

2.1. Materials

A sample of natural, terrestrial, troilite from Del Notra, California, USA, was donated by the Museum of South Australia. Powder XRD on a sample of the material confirmed it to be iron sulfide, troilite 2C = FeS. This is the standard type of troilite formed at temperatures $<$140 °C (the α-transition temperature). Acid digestion of a sample of the troilite yielded 95.9 wt. % of the material to be Fe and S together with 5.1% of other impurities. Impurities detected included Si, Al, Cu, and Ca. The Fe:S mole ratio was calculated from these results to be = 1:1.0. The result of the digestion adds support to the more definitive XRD result and is within the range of iron deficiency allowed within the definition of troilite (the limit being $Fe_{0.945}S$) (Goodenough, 1982).

Diffraction peaks other than those accounted for by troilite were present in the XRD pattern (Fig. 1) indicating the presence of other phases. Clinochlore $(Mg, Fe, Al)_6 (Si, Cr)_4 O_{10} (OH)_8$, a complex metal silicate hydroxide, was identified as a minor phase. A third, unknown phase was also detected as reflections in the low 2θ range. These peaks, while as yet unidentified, did not match any known sulfide.

The initial XPS survey of the polished troilite surface revealed (in addition to adventitious carbon) S, Fe, O, Al and a minor amount of Si to be present. The Al, Si, and O can be explained as arising from the aluminosilicate impurity as well as a contribution from Al and O from residual alumina (Al_2O_3) polishing powder. When oxygen associated with the impurities was factored out (using an Al:O ratio of 2:3) only 2–9 % of the oxygen present on the surface was bonded to surface iron or sulfur.

XRD powder studies of the material used for the polished pyrrhotite discs confirmed the material to be hexagonal pyrrhotite comprising both type 5C and 11C phases within the same sample. This sample was used in previous reported investigations (Thomas et al., 1998, 2000, 2001). The 5C and 11C phases are typical of the intermediate form of pyrrhotite, which has a continuous composition range, iron-deficient in comparison with troilite, but not as deficient as in the monoclinic, Fe_7S_8, form of pyrrhotite. The 5C and 11C phases are closely related and result from variations in the distribution of iron vacancies within the pyrrhotite structure. The composition of pyrrhotite with these phases is $Fe_{0.91}S$–$Fe_{0.90}S$. A composition of $Fe_{0.91}S$ was obtained via EDAX during SEM analysis of a polished sample.

A limited number of experiments with pyrite were done within this study. The pyrite was from Huanzala, Peru, supplied by Ward's Natural Science Establishment Inc., New York. The results of powder XRD confirmed the material to be pyrite. Analysis of an acid digest of the pyrite indicated impurities of silicate (3 wt. %), lead (0.27 wt. %) with other impurities of copper, zinc, and carbon each being less than 0.1 wt. %.

Polishing was done on sample surfaces cut with a water-cooled diamond saw. The discs were mounted with epoxy onto the end of a glass tube. The polishing was carried out in a glove bag filled with high purity oxygen free N_2. An initial wet polish was done with 1000 gauge, and then 360 gauge, silicon carbide paper. The final polishing was done dry with alumina polishing powder. The surface was then wiped, using tissues, with deoxygenated distilled water to remove loose material.

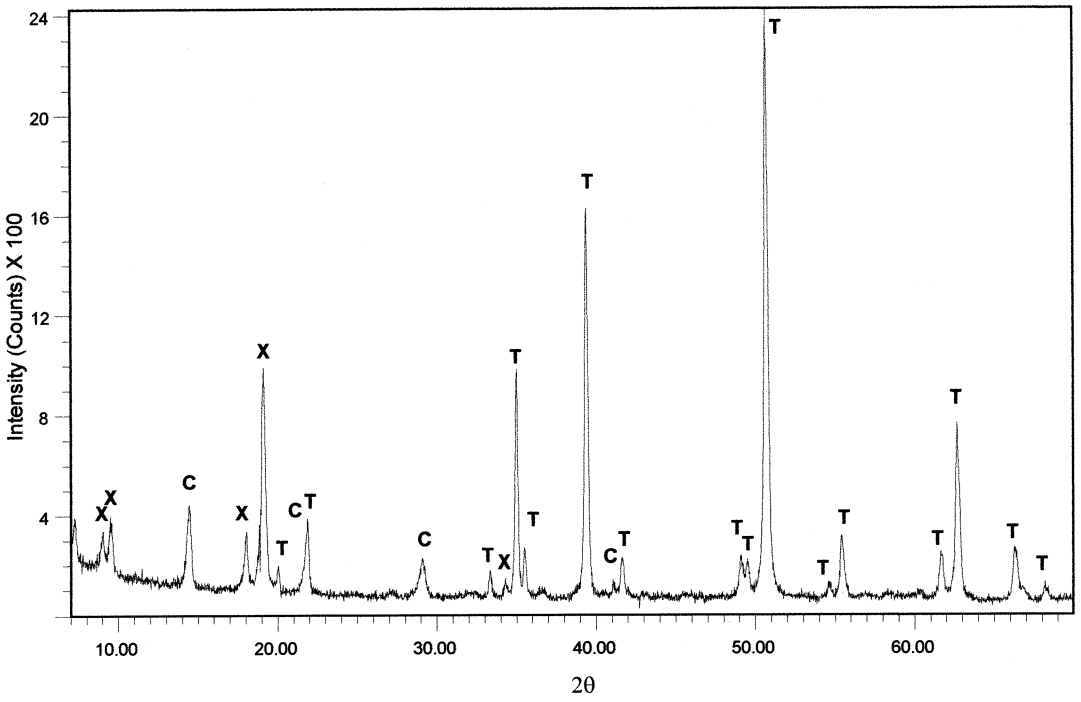

Fig. 1. XRD analysis of the troilite sample used in this study. Major diffraction peaks are due to troilite (T) and minor intensity from clinochlore (C). An unidentified, nonsulfide phase (X) is also present.

This method follows that of Cheng et al. (1993). The surface area of the polished discs was estimated geometrically.

Electrodes were made by backing an abraded disc of the material with graphite-impregnated glue and graphite impregnated webbing. The use of graphite glue, recommended by Peters (1976), eliminates contact with another metal, as in the case of conducting glue that contains silver. A tungsten rod was passed through the glass tube on which the sample was mounted and held with light pressure in the bed of webbing and glue. The electrode was polished, as described, before each use. Measuring the resistance of the system (using a Voltcraft Model 96 multimeter) checked the electrical contact.

2.2. Dissolution Conditions

The conditions for the dissolution experiments were described previously (Thomas et al., 2000). Dissolution studies were conducted in glass vessels held at a constant temperature by use of a thermostatically controlled water bath. Perchloric acid (0.1 M) was used to minimize the effects of anion adsorption onto the surface and the formation of complexed cations in solution (Pearson, 1966). Solutions were stirred at rates of 700–1000 rpm. The acid was pre-purged with Ar for at least 2 hours before each experiment and purging was maintained throughout the experiment. Reaction rates were determined by monitoring the concentration of Fe in solution. Samples were extracted, via a syringe, at timed intervals and the concentration of Fe determined by ICP–AE.

An electrode potential was applied, when required, using a WENKING model MP81 potentiostat referenced to a calomel electrode. The calomel electrode was contained within a "Quick Fit" glass sleeve (with a permeable frit in the bottom) containing 0.1 M KCl. This allowed electrical contact but minimized the diffusion of Cl^- into the perchloric acid. This system also prevented the precipitation of $KClO_4$ within the frit of the calomel electrode. The mineral electrode and the glass sinter in the outer glass sleeve of the calomel electrode were aligned in close proximity during the experiments. A platinum counter electrode was used in the system. The counter electrode consisted of a piece of Pt foil attached to a Pt wire which was sealed within a glass sleeve, with a glass sinter in the bottom, filled with 0.1 M KCl solution. This avoided products that produced interference with the system under investigation. Potential values reported in this paper have been referenced to the potential of the standard hydrogen electrode (SHE).

2.3. XPS Analysis

Polished discs of troilite, pyrrhotite or pyrite, were mounted on stubs for XPS analysis using conducting tape. Acid reacted discs were removed from the reaction vessel under N_2 and rinsed with deoxygen-

Table 1. XPS peak parameters used for S2*p* and Fe2$p_{3/2}$ chemical states fitting for troilite and pyrrhotite surfaces. Only the S2$p_{3/2}$ components are listed. Values in parentheses indicate the relative intensity contribution of components in the multiplet structure.

Chemical state	Binding energy, eV	FWHM, eV
S^{2-} (surface)	160.5	0.8*
S^{2-}	161.1	1.4
S_2^{2-}	162.5	1.4
S_n^{2-}	163.7	1.8
S^0	164.2	1.8
SO_3^{2-}	166.4	1.8
SO_4^{2-}	168.5	1.8
Fe(II)–S	706.8 (0.21)	1.3
Fe(II)–S	707.8 (0.53)	1.4
Fe(II)–S	708.5 (0.18)	1.3
Fe(II)–S Satellite	713.6 (0.09)	2.3
Fe(III)–S	709.2 (0.47)	1.6
Fe(III)–S	710.3 (0.31)	1.6
Fe(III)–S	711.3 (0.16)	1.6
Fe(III)–S	712.2 (0.06)	1.6
Fe(III)–O	710.3 (0.31)	1.8
Fe(III)–O	711.3 (0.21)	1.8
Fe(III)–O	712.4 (0.10)	1.8
Fe(III)–O	713.5 (0.04)	1.8

* Obtained with monochromatic source.

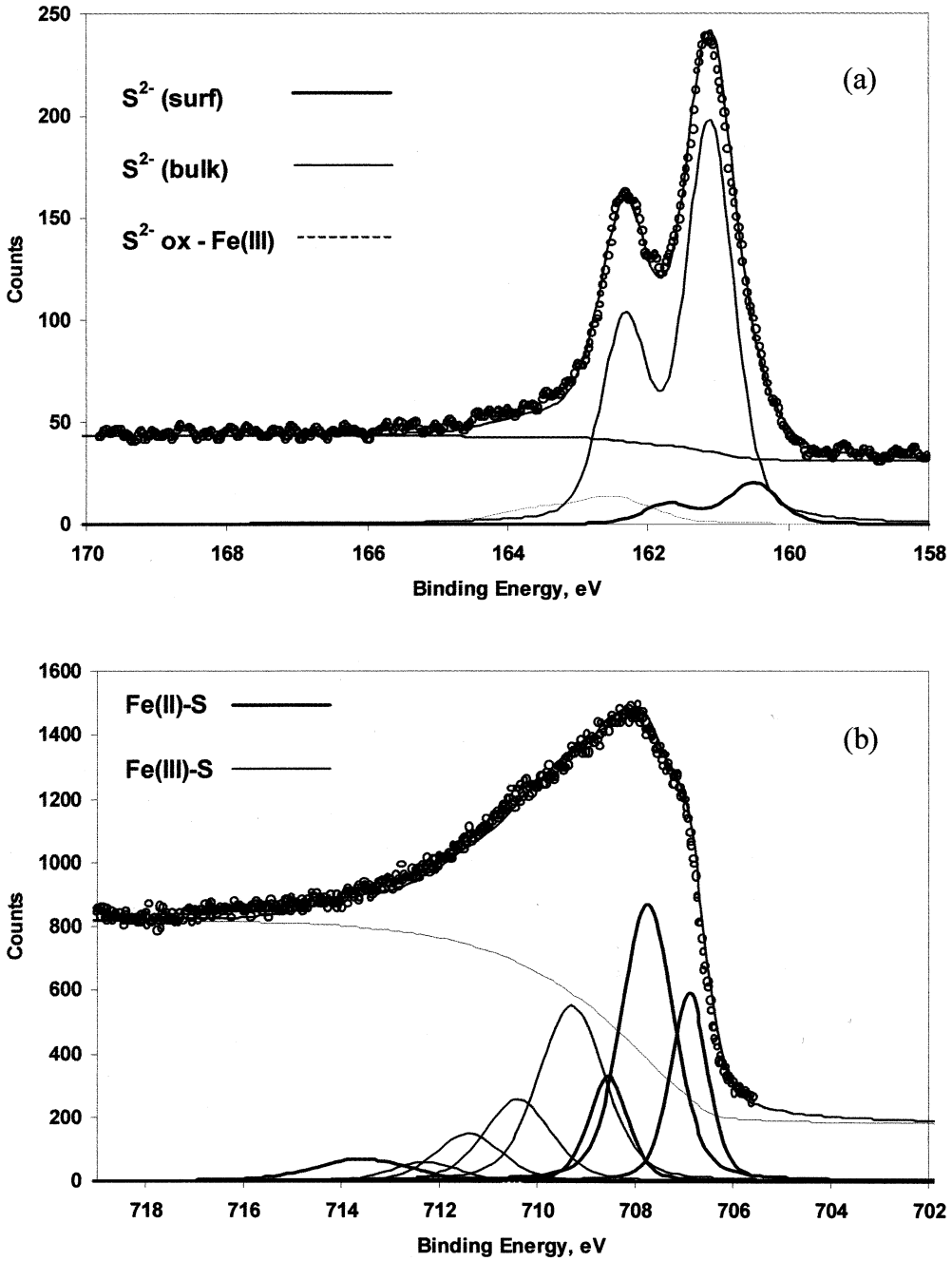

Fig. 2. Curve-fitted (a) S2*p* and (b) Fe2$p_{3/2}$ XPS regions of vacuum-fractured troilite.

ated water before mounting. Each sample was placed in a N_2 filled transfer vessel and taken for immediate analysis.

The XPS spectra of the polished and acid reacted samples were recorded using a PHI 5600ci spectrometer with a nonmonochromatized MgKα irradiation source at 300 W, using a 1 mm^2 analysis area. The analyzer pass energy was 17.9 eV. The sample stage was cooled, using liquid N_2, during analysis. In addition, the sample was step cooled in the fore-vacuum chamber, before the application of vacuum, to prevent loss of volatile species, particularly elemental sulfur (Kartio et al., 1992).

Fresh, vacuum fractured troilite was examined by XPS at CANMET, National Resources Canada, Ottawa, using a PHI 5800 spectrometer with a monochromatic AlKα source. X-ray power conditions and analysis area were 300 W and 600 $\times$ 600 μm, respectively, and the analyzer pass energy was set to 7.95 eV.

2.4. The Fitting of XPS Spectra

Peaks were referenced to the Cls peak at 284.8 eV. Each of the S2*p* states was fitted with a doublet (Pratt et al., 1994) reflecting the S2$p_{3/2}$ and S2$p_{1/2}$ components of each contribution. The binding energy (BE) separation of the S2$p_{1/2}$ doublet is 1.18 eV higher than the S2$p_{3/2}$ and is half the intensity of the S2$p_{3/2}$ peak. These constraints have been observed experimentally for metal sulfides, disulfides and sulfur and have been used successfully to fit the S2*p* spectra of polysulfide (Termes et al., 1987).

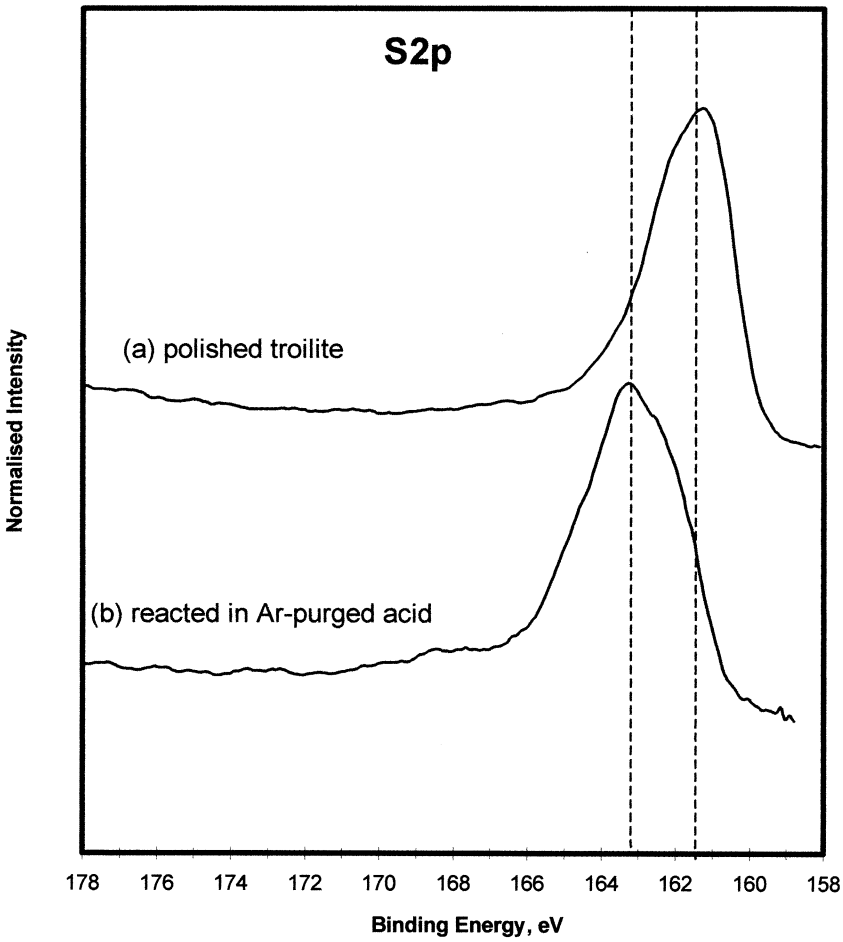

Fig. 3. The charge corrected S2*p* region for polished troilite: (a) initial surface after polishing under N_2; charge correction = 0 eV; (b) after reacting for 150 min in Ar-purged 0.1 M $HClO_4$ at 50 °C; charge correction = +0.7 eV. Note: the vertical lines indicate the maximum binding energy of each peak.

Fe2*p* states were fitted using contributions from Fe(II) and Fe(III) bonded to sulfur and Fe(III) bonded to oxygen. Fe2*p* regions were fitted after the manner of Pratt et al. (1994), who in turn based their method on the multiplet structure of states for Fe(II) and Fe(III), initially calculated (for the free ions) by Gupta and Sen (1974, 1975). This method has subsequently been used and confirmed for iron sulfide surfaces by conventional XPS (Mycroft et al., 1995; Nesbitt et al., 1998) and synchrotron radiation XPS studies (Schaufuß et al., 1998). Table 1 summarizes S2*p* and Fe2*p* binding energy assignments and peak characteristics used in this study.

3. RESULTS: PRISTINE TROILITE SURFACE (S2*p* AND Fe2*p* SPECTRA)

A troilite surface was prepared by fracturing a bulk sample under the ultrahigh vacuum within the spectrometer. The surface was sufficiently conducting that no charge correction was required. The S2*p* and Fe2$p_{3/2}$ regions obtained from the vacuum fractured troilite surface, acquired using a monochromatic AlKα source, are presented in Figures 2a and 2b. Binding energy assignments and curve fit details are given in Table 1. The major S2*p* component is situated at 161.1 eV binding energy and is assigned to the monosulfide, S^{2-} doublet. A clear shoulder to the low binding energy side of the main component is also seen which can be fitted by a small doublet at 160.5 eV binding energy comprising ~9% of the total S2*p* signal. We have assigned this component to unsatisfied monosulfide in the first monolayer of the surface, produced by the rupture of S–Fe bonds during fracture. We did not perform angle-resolved measurements to confirm the surface nature of this component however we would expect, under our analysis conditions, ~9% of the S2*p* signal to arise from the first 1–1.5 monolayers (Briggs and Seah, 1990). There is also an additional contribution(s) to higher binding energy, above the bulk monosulfide peak. We have fitted this region with a broad doublet at ~162.4 eV binding energy, consistent with the reported range of disulfide (Smart et al., 1999). This contribution comprises ~9% of the signal and is most likely due to more oxidized sulfur associated with some Fe(III) in the troilite, arising from zones of nonstoichiometry. The Fe2$p_{3/2}$ spectrum of vacuum-fractured troilite (Fig. 2b) has been fitted with the multiplet structures of high spin Fe(II) and Fe(III) after Gupta and Sen (1975) and does show a significant contribution from Fe(III)–S. Indeed Fe(III) contributes more than 40% of the Fe2$p_{3/2}$ signal. This appears to be at odds with the S2*p* result but there may be some Fe(III) contribution due to exposure of the minor phase clinochlore, although no Si signal was detected in broad scan survey

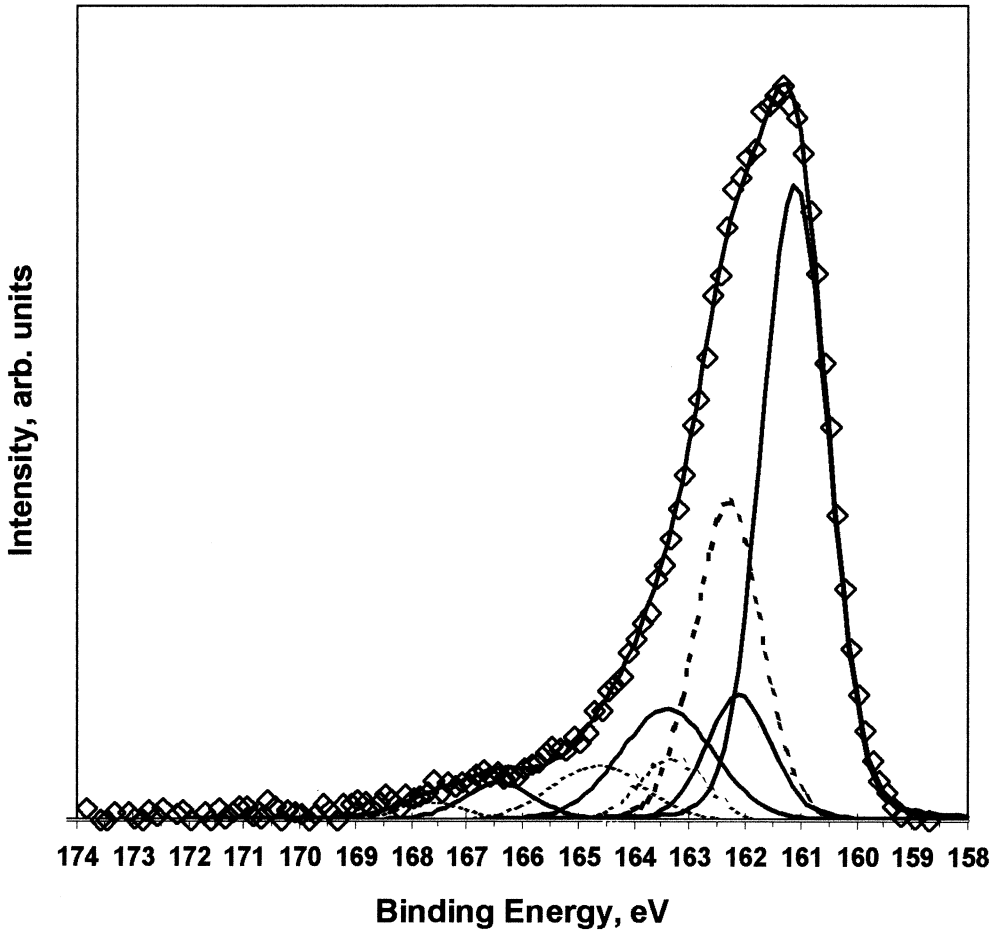

Fig. 4. Curve fit for the charge corrected S2*p* region of troilite polished under N_2.

spectra. Furthermore, attempts at fitting the pristine troilite Fe2$p_{3/2}$ guided by the S2*p* analysis and including contributions from Fe(III)–O were unable to reproduce the acquired spectrum. It is clear that a more pure sample (perhaps nonterrestrial) is required if the analysis of pristine troilite is to be taken any further.

In contrast with the S^{2-} doublet of the S2*p* region for cleaved troilite, Pratt et al. (1994), found that the S2*p* region of vacuum cleaved pyrrhotite, while containing a predominance of S^{2-}, had more significant contributions from S_2^{2-} and S_n^{2-}.

4. RESULTS: S2*p* SPECTRA OF POLISHED AND ACID REACTED SURFACES

4.1. Surfaces Polished Under N_2

4.1.1. Troilite

The polished troilite surface required no charge correction, the Cls peak occurring at 284.8 eV. The S2*p* region of the polished troilite surface [Fig. 3, curve (a)] has a peak maximum at 161.8 eV. The S2*p* region from the polished surface can be fitted with 63% from the S^{2-} doublet, 16% from disulfide S_2^{2-} and 17% attributed to polysulfide (S_n^{2-}). A minor proportion (4%) of the peak area can be assigned to oxysulfur species (the BE is not high enough for sulfate). The fitting is shown in Figure 4 and summarized in Table 2.

4.1.2. Pyrrhotite

The surface of the polished pyrrhotite examined showed that charge correction was necessary, as gauged by the position of the C1s peak. Displacement to a BE 0.7 eV lower than 284.8 eV was observed. This observation and the implications for the dissolution mechanism of pyrrhotite have been discussed in an

Table 2. A summary of the species contributing to the S2*p* region as determined by curve fitting of results from XPS analysis. The fit for each surface accounts for 100 ± 5 % of the collected signal.

Species (% of S2*p* signal)	S^{2-}	S_2^{2-}	S_n^{2-}	S^0	SO_3^{2-}	SO_4^{2-}
Vacuum cleaved troilite	89	11				
Vacuum cleaved pyrrhotite, Pratt et al. (1994)	76	11	13			
Initial polished surface troilite	63	16	17		4	
Initial polished surface pyrrhotite	57	28	15			
Troilite after reaction in Ar-purged acid	12	22	49		8	8
Pyrrhotite after reaction in Ar-purged acid	7	42	37	9	5	

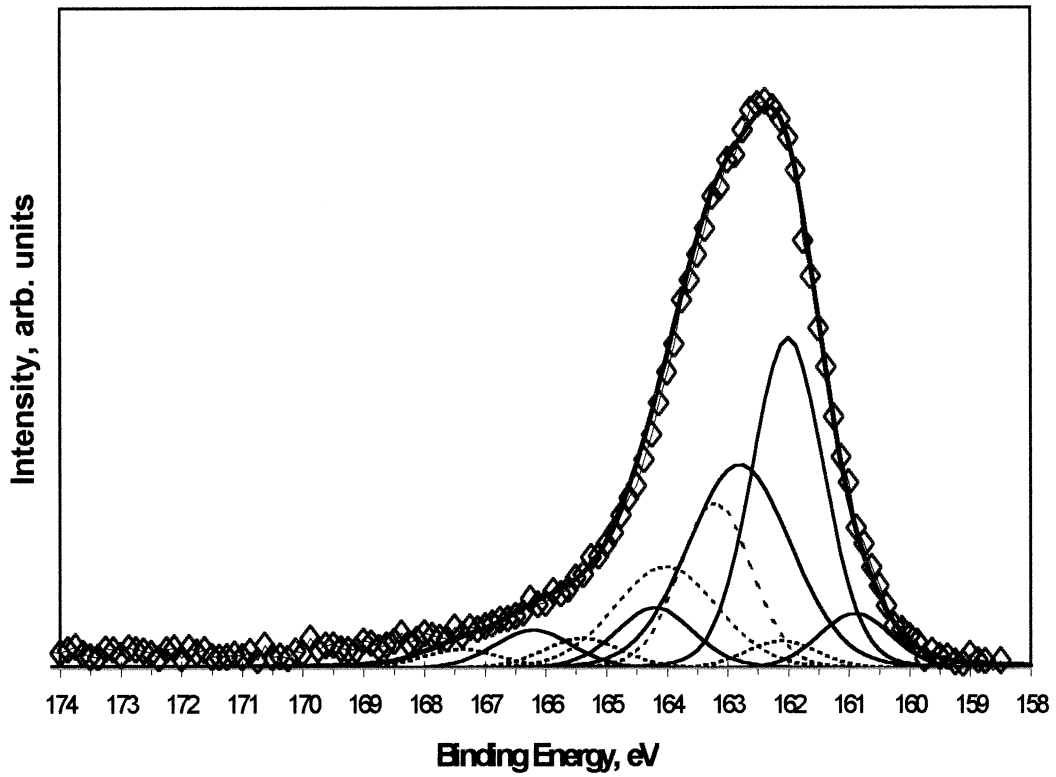

Fig. 5. A curve fit of the S2*p* peak obtained from a polished pyrrhotite surface, after reaction in Ar-purged 0.1 M perchloric acid at 50°C for 150 minutes.

earlier paper (Thomas et al., 2001). The fit of the S2*p* region was predominantly S^{2-}, with S_2^{2-} and S_n^{2-} (as summarized in Table 2). The sulfur species on the surface of the polished pyrrhotite was similar in nature to that found by Pratt et al. (1994) on pyrrhotite (of closely related composition) cleaved under vacuum (Table 2). The major contribution to the S2*p* region of both surfaces was monosulfide.

4.1.3. Pyrite

No surface charge correction was needed when analyzing the polished pyrite. The S2*p* region (not shown) had a single peak with the BE maximum at 162.7 eV, assigned to S_2^{2-}. There was some evidence of the disulfide doublet but it was not clearly defined, due in part to the nonmonochromatic radiation used.

4.2. Surfaces Reacted in Ar-Purged Acid at 50 °C

4.2.1. Troilite

The troilite, reacted in Ar-purged acid for 150 minutes, required a charge correction of 0.7 eV, to higher binding energy (the maximum binding energy of the Cls peak occurring at 284.1 eV). The S2*p* region after reaction in acid is shown in Figure 3, curve (b). The S2*p* fit obtained (see Table 2) shows increased oxidation of the sulfur compared with the initial surface. The S^{2-} signal decreases dramatically after reaction in the acid, compared with the initial polished surface, with the predominant sulfur signal coming from polysulfide, S_n^2.

4.2.2. Pyrrhotite

The fit of the S2*p* spectrum obtained from pyrrhotite reacted in Ar-purged perchloric acid for 150 minutes is shown in Figure 5 and summarized in Table 2. The S^{2-} signal decreased dramatically from 57% on the initial polished surface to 7%, after reaction in the acid. The predominant signal becomes disulfide S_2^{2-}, at 42%. There is also a major contribution (37%) from polysulfide, S_n^{2-}, and a minor contribution from elemental sulfur.

4.2.3. Pyrite

The S2*p* spectra obtained from pyrite after reaction in acid for 60 minutes (and also a spectrum obtained after reacting overnight for 10 hours) was the same as that obtained from the initial polished surface, with a peak maximum at 162.7 eV, assigned to S_2^{2-} (see Table 2). These spectra are not shown.

5. RESULTS: Fe2*p* SPECTRA OF POLISHED AND ACID-REACTED SURFACES

5.1. Surfaces Polished Under N_2

5.1.1. Troilite

The $Fe2p_{3/2}$ region of the polished troilite surface (Fig. 6b) shows both Fe(II)–S (38%) and Fe(III)–S (43%) with a more minor contribution from Fe(III)–O (19%) (Table 3). The Fe(III)–O is not unexpected since Fe(III)–S states are observed on the surface. Fe(III)–S could react in the presence of H_2O

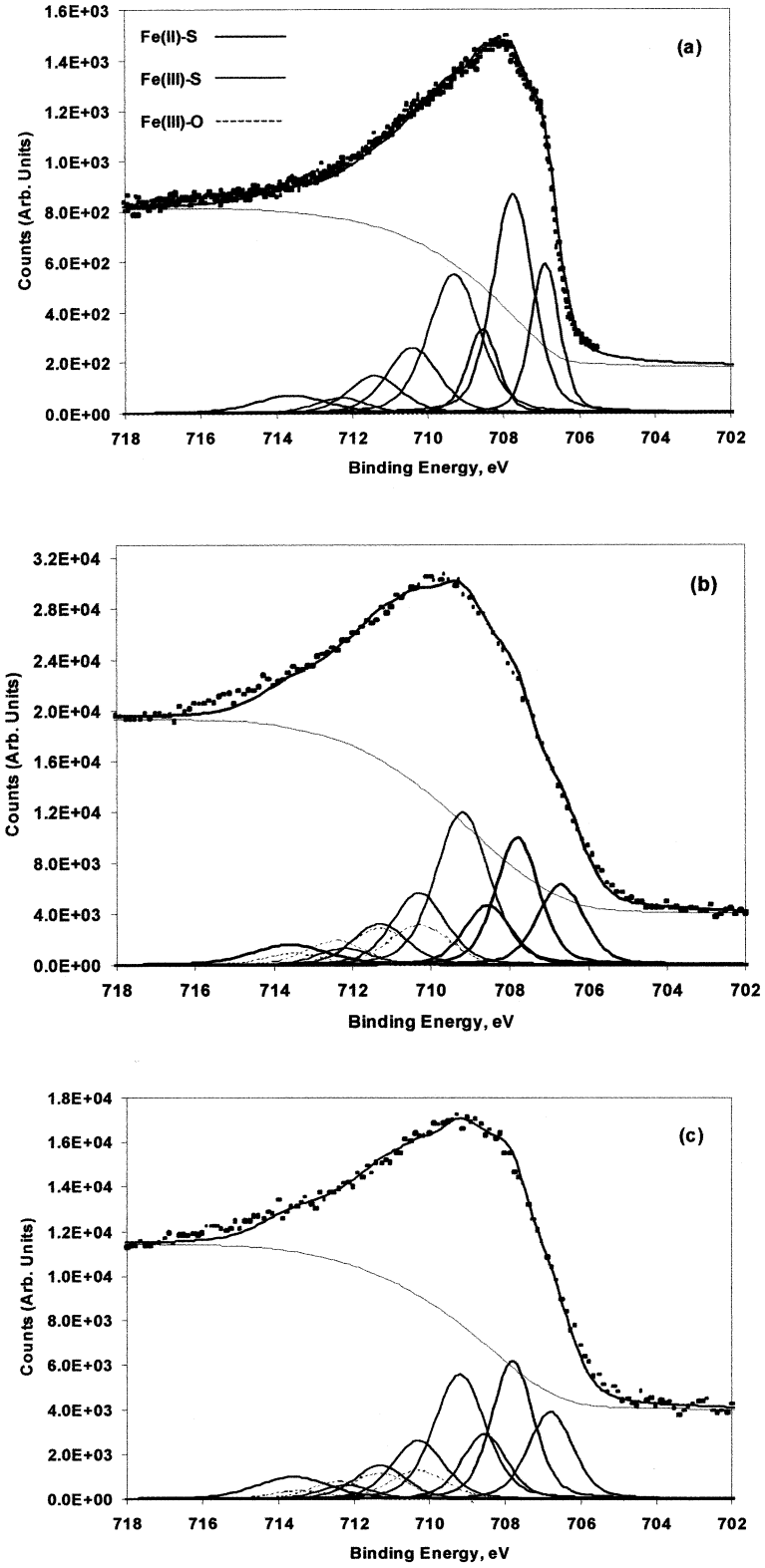

Fig. 6. Peak fitting of the Fe2$p_{3/2}$ signals from (a) vacuum fractured troilite, (b) polished troilite, and (c) polished pyrrhotite, showing contributions from Fe(II)–S, Fe(III)–S, and Fe(III)–O.

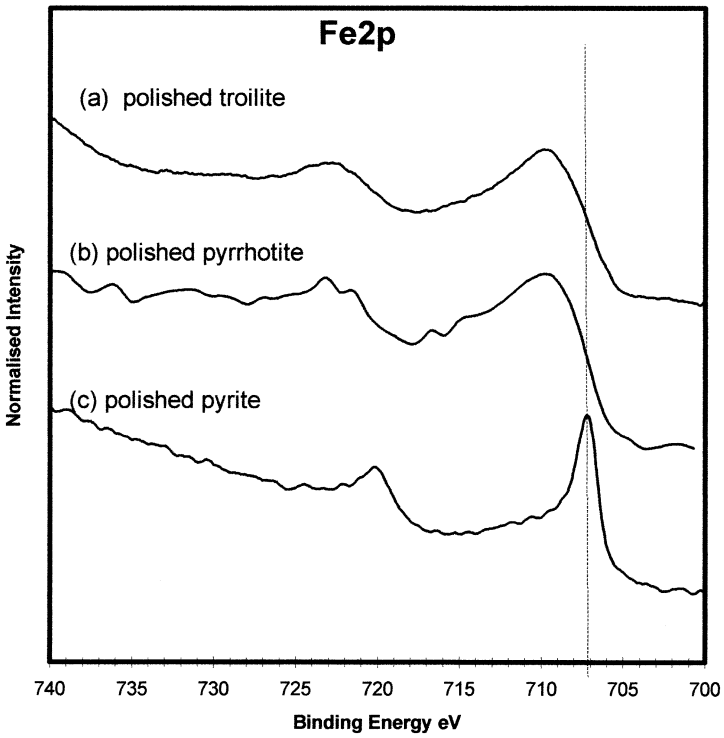

Fig. 7. A comparison of the charge corrected Fe2*p* region of samples polished under N_2 (a) troilite, (b) pyrrhotite, (c) pyrite. Note: the vertical line indicates the Fe(II)–S binding energy (obtained from pyrite).

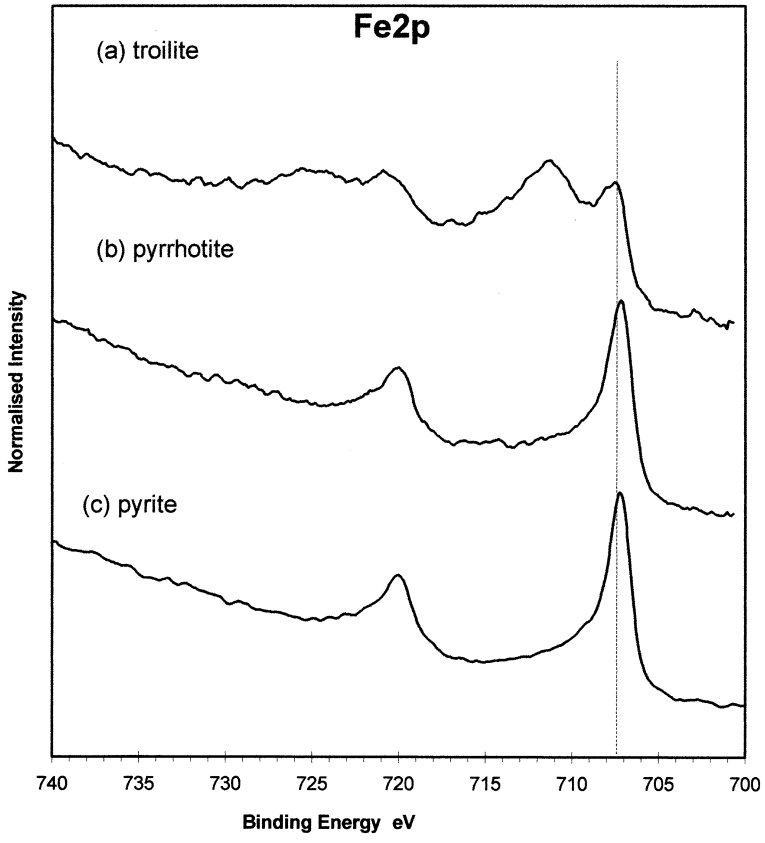

Fig. 8. A comparison of the charge corrected Fe2*p* regions of polished samples after reaction in Ar-purged acid: (a) troilite reacted 150 min; charge correction = +0.7 eV, (b) pyrrhotite reacted 150 min; charge correction = +0.7 eV, (c) pyrite reacted 60 min; no charge correction required. Note: the vertical line indicates the Fe(II)–S binding energy.

Table 3. A summary of the species contributing to the Fe2p3/2 region, as determined by curve fitting of results from XPS analysis. The fit for each surface accounts for 100 ± 5 % of the collected signal.

Species (% of Fe2*p*3/2 signal)	Fe(II)–S	Fe(III)–S	Fe(III)–O
Vacuum cleaved troilite	56	44	
Vacuum cleaved pyrrhotite, Pratt et al. (1994)	68	32	
Initial polished surface troilite	38	43	19
Initial polished surface pyrrhotite	46	39	15
Troilite after reaction in Ar-purged acid	41	21	38

(liquid or vapor) to form Fe(III)–O. Water was not excluded during the polishing procedure.

5.1.2. Pyrrhotite

The Fe2$p_{3/2}$ region of polished pyrrhotite [Fig. 6, curve (c)], has a fit very close to that of vacuum cleaved pyrrhotite, reported by Pratt et al. (1994), but with some minor contribution from Fe(III)–O. [Pratt et al. (1994) were the first to identify Fe(III)–S as well as Fe(II)–S bonding on a pyrrhotite surface cleaved under vacuum, and thus free of oxygen]. A summary of the fit from the polished material and the fit of Pratt et al for the vacuum cleaved surface is given in Table 3. The contribution from Fe(III)–O on the polished surface is not unexpected since Fe(III)–S states on the surface could react in the presence of H_2O (liquid or vapor) to form Fe(III)–O. Water was not excluded during the polishing procedure.

5.1.3. Pyrite

Unlike the polished surfaces of troilite or pyrrhotite, the Fe2$p_{3/2}$ region of polished pyrite [Fig. 7 curve (c)], showed a sharp peak at 707.2 eV. Nesbitt et al. (1998) obtained a peak maximum at 707.0 eV on vacuum fractured pyrite. Fitting of the peak in this and other studies shows the domination of Fe(II)–S. There was no evidence of Fe(III)–O (Nesbit et al., 1998; Nesbit and Muir, 1994).

5.1.4. Comparison of the Fe2p spectra of polished troilite, pyrrhotite, and pyrite

Figure 7 compares the Fe2*p* regions of polished surfaces of troilite, pyrrhotite, and pyrite. The similarity between the troilite and pyrrhotite surfaces is evident. The figure shows clearly the significant difference between these surfaces and that of pyrite [which is dominated by Fe(II)–S]. The Fe2$p_{3/2}$ regions for the troilite and pyrrhotite are broad due to the presence of both Fe(III)–S and Fe(II)–S but pyrite has a sharp peak at 707.2 eV indicating Fe(II)–S (as discussed in Sections 4.2.2–4.2.3).

5.2. Surfaces Reacted in Ar-Purged Acid at 50 °C

5.2.1. Troilite

The Fe2$p_{3/2}$ region of the troilite surface reacted in acid for 150 minutes [Fig. 8, curve (a)] shows contributions from Fe(II)–S, Fe(III)–S, and Fe(III)–O. The curve fit of this peak is summarized in Table 3. The most significant change is distinct peaks at 707.5–708 eV [Fe(II)–S] and 711 eV [Fe(III)–O], with relatively less contribution in the region of 709–709.5 eV [Fe(III)–S].

5.2.2. Pyrrhotite

After pyrrhotite has reacted for 150 min in Ar-purged acid, Figure 8, curve (b) shows that the Fe2$p_{3/2}$ region of pyrrhotite has become similar to that of pyrite [Fig. 8, curve (c)], rather than troilite [Fig. 8, curve (a)]. A pyrrhotite surface reacted for 70 min was also examined (not shown). At 70 min the Fe2$p_{3/2}$ region showed a close resemblance to the initial polished surface; only a reduction in Fe(III)–O was noted. In the period from 70 min to 150 min the Fe2$p_{3/2}$ region changed dramatically, with an increase in the signal due to Fe(III)–S and a decrease in the signal at 709.5 eV [Fig. 8, curve (b)]. It is proposed that the change was due to a decrease of Fe(III)–S, with alteration to Fe(II)–S. [Fe(II)–O was not considered as contributing to the 709.5 eV signal in view of the soluble nature of Fe(II)–O oxides and the exposure time of the surface to the Ar-purged acid.]

5.2.3. Pyrite

The Fe2*p* spectrum of pyrite, shown in Figure 8, curve (c), was obtained after reaction for 60 min in Ar-purged acid. The spectrum shows minimal change from the spectrum of the polished surface [Fig. 7, curve (c)].

5.2.4. Comparison of the Fe2p regions of Ar-purged acid reacted troilite, pyrrhotite, and pyrite

Figure 8 compares the Fe2*p* regions of polished surfaces of troilite [curve (a)], pyrrhotite [curve (b)], and pyrite [curve (c)]. The similarity between the troilite and pyrrhotite surfaces, evident on the initial surface (see Fig. 7), has changed dramatically after reaction for 150 min in pH 1 Ar-purged acid. The Fe in the acid reacted surface of pyrrhotite is now very similar to that of pyrite [which is dominated by Fe(II)–S, as indicated by the peak at 707.2 eV].

6. RESULTS: THE DISSOLUTION OF IRON SULFIDES, IN Ar-PURGED ACID, IN RESPONSE TO APPLIED POTENTIAL

It was hypothesized that application of a cathodic potential to a troilite electrode immersed in acid would increase the rate of dissolution of the troilite potential (by reducing S–S covalent interactions to S^{2-} ions). This was based on the observations from XPS surface analysis of polished troilite, that showed the S2*p* region to have low levels of polysulfide (S_n^{2-}) with the amount increasing after dissolution in Ar-purged acid (see Table 2). The effect of applied potential on the dissolution of troilite in Ar-purged acid is shown in Figure 9. The dissolution of the troilite was monitored by periodic analysis of the Fe in solution. The solution data was converted to an average rate over the period between sampling and this was plotted as a function of time and electrode potential.

The initial increase in the rate of Fe release, in the period before the application of a potential, was due to the effect of

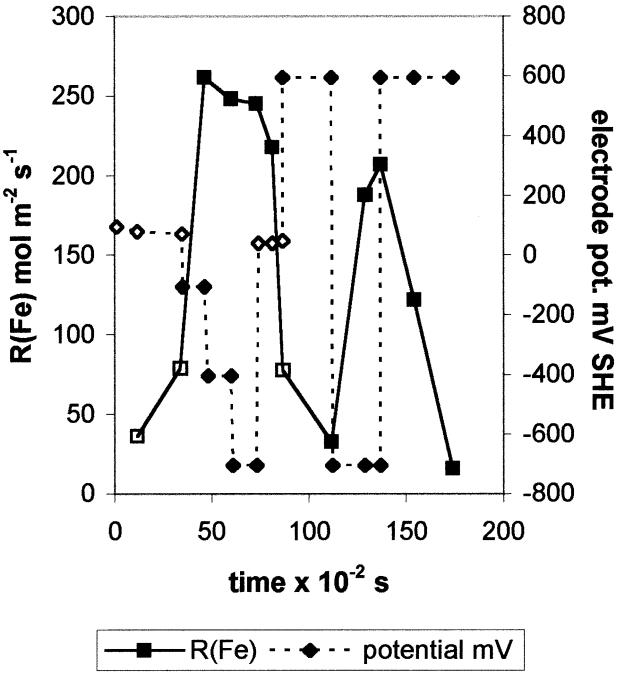

Fig. 9. The change in the rate of release of Fe^{2+} [*R*(Fe)] from a troilite electrode, in 0.1 M Ar-purged perchloric acid at 50 °C. The *R*(Fe) is shown as a function of time and as related to the potential applied to the electrode. The nonfilled symbol □ indicates the rate measured when no potential was applied (open circuit). The nonfilled symbol ◇ indicates the open circuit potential of the troilite.

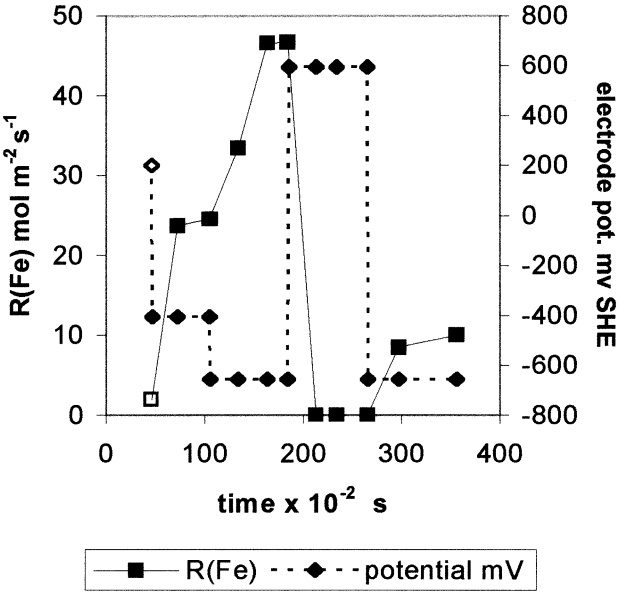

Fig. 10. The change in the rate of release of Fe^{2+} [*R*(Fe)] from a pyrrhotite electrode, in 0.1 M Ar-purged perchloric acid at 50 °C. The *R*(Fe) is shown as a function of time and as related to the potential applied to the electrode. The nonfilled symbol □ indicates the rate measured when no potential was applied (open circuit). The nonfilled symbol ◇ indicates the open circuit potential of the pyrrhotite.

oxidized species on the initial troilite surface. With the application of −105 mV, the rate of dissolution (as indicated by the rate of release of iron into solution) increased by a factor of 3.5, thus electrochemical reduction had occurred. Further decreases in potential (to −405 mV and then −705 mV) resulted in very little change in rate. To check if the increase in rate with the application of potential was due to the removal of a passivating surface layer, the applied potential was turned off. The rate returned to the value recorded immediately before the application of the cathodic potential, demonstrating that the effect was not due to the removal of a surface layer.

Application of an anodic potential (595 mV for 2500 s) caused the dissolution rate to decrease to a value similar to that measured immediately after the material was placed in the acid, consistent with the formation of an oxidized surface layer. The application of a cathodic potential of −705 mV increased the dissolution rate to a value similar to that obtained previously at this potential. Thus changes caused by the anodic potential were in the most part reversible (as shown in Fig. 9).

The pattern of response of the dissolution rate of pyrrhotite to applied cathodic potential (Fig. 10) differed from that of troilite (Fig. 9). Stepwise lowering of the potential to −705 mV resulted in an increased rate of dissolution with each step. At −705 mV the rate had almost reached the rate obtained with troilite with no applied potential.

After the application of −705 mV to pyrrhotite for a period of time, an immediate change was made to an anodic potential of 595 mV. The anodic potential rapidly decreased the dissolution rate to a level where there was no observable increase of iron in solution (within 1500 s) (Fig. 10). This differed from the results obtained using troilite, where an anodic potential of the same magnitude applied for 2500 s decreased the rate to the level obtained with no applied potential. Reapplication of a cathodic potential of −705 mV to the pyrrhotite caused only minor increase in dissolution rate compared with the first application of this potential. Thus, unlike troilite, the changes in the pyrrhotite surface were more resistant to being reversed.

In contrast to pyrrhotite and troilite, pyrite can only dissolve in acid with the production of HS^- or H_2S if a sufficiently cathodic potential is applied.

7. CONCLUSIONS

The XPS examination of a pristine troilite surface is to our knowledge the first of its kind to be published. However, more detailed measurements need to be performed to verify and complete our interpretation beyond that required for the present work. Particular emphasis needs to be placed on the origin and relative contributions from Fe(III) in the troilite surface layers, whether from bulk nonstoichiometry or from rupture of Fe–S bonds as in pyrite (Schaufuß et al., 1998). A comparison of troilite samples of terrestrial and lunar origin is planned for the near future to investigate stoichiometry effects. This work will concentrate on the near surface through the use of angle resolved XPS and synchrotron XPS.

In the case of pyrrhotite, both the S2*p* region of a surface fractured under vacuum (Pratt et al., 1994) and of a polished surface, show monosulfide, disulfide, and polysulfide, typical of a sulfur deficient surface. This is as expected in view of pyrrhotite being iron deficient. The polished surface of troilite and of pyrrhotite each exhibit an increased level of oxidation,

as compared with the pristine surface. This was indicated in the XPS spectra of the S2*p* and Fe2$p_{3/2}$ regions.

The results of the experiments with a cathodic potential applied to troilite in deoxygenated acid support the XPS evidence of limited S–S covalent interactions within troilite. The extent of the S–S interaction was limited, especially in comparison with pyrrhotite, since decreases in potential below −105 mV did not result in further increases in the dissolution rate.

The response of the troilite and pyrrhotite electrodes to an anodic potential (after a period of applied cathodic potential) differed. In the case of troilite the rate of Fe release decreased to the level observed with no applied potential, but with pyrrhotite the anodic potential decreased the dissolution rate such that there was no observable increase of Fe in solution over an equivalent period of time. It was also found that the changes to the pyrrhotite surface caused by the anodic potential were more resistant to being reversed, by application of a cathodic potential, than those on troilite.

The reaction of troilite, and of pyrrhotite, in Ar-purged acid (with no application of potential) increased the oxidation of the sulfur in the surface layers of both troilite and pyrrhotite. The S^2 component of the S2*p* spectrum for each dropped dramatically, accompanied by increased components for di- and polysulfides. This was not the case with pyrite, where little or no change was observed in the S2*p* or the Fe2*p* signal.

Pyrite dissolves in acid via oxidation of di-sulfide to sulfate (Eqn. 2). The S2*p* region of the acid-reacted pyrite surface showed little or no change, indicating uniform removal of iron and sulfate from the surface.

In the case of troilite reacted in Ar-purged acid, the surface became iron deficient with greatly decreased monosulfide (S^{2-}) (from 63% to 12%) and increased di- and polysulfide (S^{2-}, S_n^{2-}) (from 33% to 71%) becoming the largest contribution. Such changes would not be observed if stoichiometric, ionic dissolution (Eqn. 1) was occurring uniformly over the surface. The increase in these species after dissolution in Ar-purged acid indicates the occurrence of oxidative dissolution to form higher order polysulfides (Eqn. 3). The XPS results are supported by the electrochemical results showing that an input of electrons increased the dissolution rate in Ar-purged acid (by increasing the dissolution via Eqn. 1),

$$FeS - FeS_n \rightarrow Fe^{++} + FeS_{n+1} + 2e^-. \quad (3)$$

Further evidence for the surface of the troilite reacted in Ar-purged acid becoming more like that of pyrrhotite was the change in the observed charge shift during XPS analysis. The cleaved surface and the polished surface each required no charge shift correction, the C1s peak occurring at 284.8 eV. However, the acid-reacted surface of troilite required a charge correction of 0.7 eV to higher binding energy, the same as was observed for the initial polished pyrrhotite surface and the acid-reacted pyrrhotite surface.

The surface of pyrrhotite was greatly changed by reaction in Ar-purged acid. After reacting for 150 minutes, the monosulfide contribution to the S2*p* peak decreased from 57% on the initial polished surface to 7%. Disulfide became the predominant contributor to the S2*p* region (42%). The most dramatic change for this surface was in the XPS Fe2*p* spectra. After 150 minutes, the Fe2$p_{3/2}$ region was dominated by a peak at 707 eV, Fe(II)–S, with almost total elimination of contributions in the region of 709.5–710.3 eV. It is proposed that the change was due to a decrease of Fe(III)–S, with alteration to Fe(II)–S. Figure 8 shows clearly the close resemblance of the Fe2$p_{3/2}$ region of the acid-reacted pyrrhotite [curve (b)] to that of pyrite [curve (c)]. The changes in the Fe2*p* spectrum and the S2*p* spectrum indicate this acid reacted surface being dominated by di-sulfide, rather than mono-sulfide.

The nature of the changes to both the Fe2$p_{3/2}$ and S2*p* regions of pyrrhotite reacted in acid for 150 minutes supports the contention that restructuring to a pyrite-like structure has occurred with pyrrhotite. Such a restructuring is not indicated for the acid-reacted troilite surface (reacted over the same period of time). The observed changes to the pyrrhotite surface support the XRD evidence of Jones et al. (1992) which showed restructuring of synthetic pyrrhotite, after reaction in Ar-purged acid at the same temperature, to an intermediate tetragonal Fe_2S_3 structure, based on a disordered form of pyrite.

Acknowledgments—The troilite used was supplied courtesy of Dr. A. Pring of the Museum of South Australia. We gratefully acknowledge the assistance of Dr. Allen Pratt of the Minerals and Metals Sector of CANMET, Natural Resources Canada, in obtaining vacuum-fractured troilite XPS spectra. In particular we acknowledge the input of Professor H. W. Nesbitt, which helped us to focus the paper.

Associate editor: D. Sparks

REFERENCES

Bertaut E. F. (1956) Structure de FeS stoichiometrique. *Bull. Soc. Fr. Mineral. Cristallogr.* **79,** 276–292.

Briggs D. and Seah M. P. (Eds.), (1990) *Practical Surface Analysis by Auger and X-ray Photoelectron Spectroscopy*, p. 183; Wiley.

Cheng X., Iwasaki I., and Smith K.A. (1993) An electrochemical study on cathodic decomposition behaviour of pyrrhotite in deoxygenated solutions. *Miner. Metall. Process.* **11,** 40–47.

Evans H. T. (1970) Lunar troilite: Crystallography. *Science* **167,** 621–623.

Fleet M. E. (1978) The pyrrhotite–marcasite transformation. *Can. Mineral.* **16,** 31–35.

Goodenough J. B. (1982) Iron sulfides. *Ann. Chim. Fr.* **7,** 489–504.

Gupta R. P. and Sen S. K. (1974) Calculation of multiplet structure of core *p*-vacancy levels. *Phys. Rev. B.* **10,** 71–79.

Gupta R. P. and Sen S. K. (1975) Calculation of multiplet structure of core *p*-vacancy levels. II. *Phys. Rev. B* **12,** 15–19.

Jones C. F., LeCount S., Smart R. St.C., and White T. J. (1992) Composition and structural alteration of pyrrhotite surfaces in solution: XPS and XRD studies. *Appl. Surf. Sci.* **55,** 65–85.

Kartio I., Laajalehto K., Suoninen E., Karthe S., and Szargan R. (1992) Technique for XPS measurement of volatile absorbed layers: Application to studies of sulfide flotation. *SIA, Surf. Interface Anal.* **18,** 807–810.

Kostov I. and Minceva-Stefanova J. (1982) *Sulfide Minerals: Crystal Chemistry, Parageneses and Systematics*, pp. 11–31. E. Bulgarian Acad. Sci. Inst. Geol.

Mycroft J. R., Nesbitt H. W., and Pratt A. R. (1995) X-ray photoelectron and Auger electron spectroscopy of air-oxidised pyrrhotite: Distribution of oxidised species with depth. *Geochim. Cosmochim. Acta* **59,** 721–733.

Nesbitt H. W. and Muir J. J. (1994) X-ray photoelectron spectroscopic study of a pristine pyrite surface reacted with water vapour and air. *Geochim. Cosmochim. Acta* **58-21,** 4667–4678.

Nesbitt H. W., Bancroft G. M., Pratt A. R., and Scaini M. J. (1998) Sulfur and iron surface states on fractured pyrite surfaces. *Am. Mineral.* **83,** 1067–1076.

Pearson G. S. (1966) Perchloric acid. *Adv. Inorg. Chem. Radiochem.* **8,** 177–224.

Peters E. (1977) The electrochemistry of sulfide minerals. In *Trends in Electrochemistry* (ed. J.O.M. Bockris et al.), pp. 267–290. Plenum Press, NY.

Posfai M. and Dodony I. (1990) Pyrrhotite superstructures. Part I: Fundamental structures of the NC (N = 2,3,4 & 5) type. *Eur. J. Mineral.* **2,** 525–528.

Pratt A. R., Muir I. J., and Nebitt H. W. (1994) X-ray photoelectron and Auger electron studies of pyrrhotite and mechanism of air oxidation. *Geochim. Cosmochim. Acta* **58,** 827–841.

Rickard T. D. (1974) Kinetics and mechanism of the sulfidation of goethite. *Am. J. Sci.* **274,** 941–952.

Rickard T. D. (1975) Kinetics and mechanism of the sulfidation of goethite. *Am. J. Sci.* **275,** 636–652.

Schaufuß A. G., Nesbitt H. W., Kartio I., Laajalehto K., Bancroft G. M., and Szargan R. (1998) Incipient oxidation of fractured pyrite surfaces in air. *J. Electron Spectrosc. Relat. Phenom.* **96,** 69–82.

Smart R. St. C., Skinner W. M., and Gerson A. R. (1999) XPS of sulphide mineral surfaces: Metal-deficient, polysulphides, defects and elemental sulphur. *SIA, Surf. Interface Anal.* **28,** 101–105.

Termes S. C., Buckley A. N., and Gillard R. D. (1987) 2p electron binding energies for the sulfur atoms in metal polysulfides. *Inorg. Chim. Acta* **126,** 79–82.

Thomas J. E., Skinner W. M., and Smart R. St. C. (2001) A mechanism to explain sudden changes in rates and products for pyrrhotite dissolution in acid solution. *Geochim. Cosmochim. Acta* **65,** 1–12.

Thomas J. E., Smart R. St. C., and Skinner W. M. (2000) Kinetic factors for oxidative and non-oxidative dissolution of iron sulfides. *Minerals Eng.* **13,** 1149–1159.

Thomas J. E., Jones C. F., Skinner W. M., and Smart R. St. C. (1998) The role of surface sulfur species in the inhibition of pyrrhotite dissolution in acid solution. *Geochim. Cosmochim Acta* **65,** 1–12.

Tokonami M., Nisihiguchi K., and Morimoto N. (1972) Crystal structure of monoclinic pyrrhotite (Fe_7S_8). *Am. Mineral.* **57,** 1066–1080.

Vaughan D. J., Craig J. R. (1978) *Mineral Chemistry of Metal Sulfides.* Cambridge Univ. Press.